Study on the Radial Sectional Velocity Distribution and Wall Shear Stress Associated With Carotid Artery Stenosis

Zhiyong Song
University of Science and Technology Beijing
Pengrui Zhu
University of Science and Technology Beijing
Lianzhi Yang
University of Science and Technology Beijing
Zhaohui Liu
Hainan General Hospital
Hua Li
University of Science and Technology Beijing
Ruonan Li
rnli@rcees.ac.cn

Chinese Academy of Sciences Beijing
Weiyao Zhu
University of Science and Technology Beijing

Research Article

Keywords: atherosclerotic, carotid artery stenosis, haemodynamic, velocity distribution form, wall shear stress

Posted Date: December 13th, 2021

DOI: https://doi.org/10.21203/rs.3.rs-1138479/v1

Additional Declarations: No competing interests reported.

Version of Record: A version of this preprint was published at Physics of Fluids on May 1st, 2022. See the published version at https://doi.org/10.1063/5.0085796.

Abstract

Background

Atherosclerosis is an important cause of cardiovascular disease. The wall shear stress (WSS) is one of the key factors of plaque formation and dislodgement. Currently, WSS estimation is based on measurement of the blood velocity gradient. However, due to the lack of flow field measurements in carotid stenosis vessels, the two distribution forms (parabolic and non-parabolic) commonly considered in numerical simulations could cause WSS estimates to differ by more than 40%, which could seriously affect the accuracy of mechanical analysis.

Methods

This study was the first to apply 3D printing technology to create an experimental model of real-structure carotid arteries. Microparticle image velocimetry (micro-PIV) was adopted to comprehensively measure blood velocity field data at the stenosis location, providing experimental validation of numerical simulation (Fluent; finite volume method) results. Then, the flow field was simulated at a normal human heart rate (45-120 beats per minute).

Results

This study revealed that when blood flowed across the carotid artery stenosis location, the velocity distribution was not parabolic but rather a plateau-shaped distribution, with a similar flow velocity in the central area (more than 65% of the total flow path). The WSS values calculated based on a parabolic velocity distribution and the maximum velocity were nearly 60% lower.

Conclusion

This study provides a reliable method for WSS determination to better understand the vascular stenosis location and facilitate flow and shear force field research. In the future, it is necessary to carry out in-depth research on the relationship between the plaque shape, flow field distribution and WSS, and amendments to the calculated WSS for clinical stenosis should be proposed.

Background

Atherosclerosis is an important pathogenic factor of cardiovascular disease. Formation of atherosclerotic plaques on the wall of blood vessels could lead to narrowing of blood flow pathways and even blood supply obstacles. Upon plaque dislodgement, serious consequences can occur, such as cerebral haemorrhage and stroke [1-4]. Animal experiments and clinical data studies have pointed out that haemodynamic characteristics, especially the blood flow wall shear stress (WSS), are key factors leading to arterial intimal thickening, plaque growth, and stroke [5].

At this stage, the WSS is indirectly calculated based on blood flow rate measurements. The peak blood flow velocity (V_{max}) in vivo has been measured mainly via magnetic resonance phase-contrast magnetic resonance imaging (PC-MRI) and ultrasound Doppler velocimetry (spatial resolution: 0.5-1 mm). Then, assuming that the velocity distribution in the blood vessel section is parabolic, the WSS has been indirectly calculated based on the maximum speed and vessel radius considering the law of Newton inner friction [6-9].

Therefore, whether the blood flow velocity conforms to a parabolic distribution is one of the key links in terms of the accuracy of WSS calculations. Due to the low spatial resolution (0.5-1 mm) of the PC-MRI and ultrasound Doppler velocimetry techniques, blood vessel-related flow field information cannot be fully measured, so it remains difficult to reveal the characteristics of the flow velocity distribution [6,9-10]. A higher-resolution velocimetry technique, namely, echo particle image velocimetry (echo-PIV, spatial resolution up to 0.5 mm), has been employed to study the flow field distribution in a healthy carotid artery (diameter of 10 mm) in vitro, thus verifying parabolic distribution features [9]. In regard to carotid artery stenosis (only 1-3 mm in diameter) caused by plaques, this technology still cannot meet accuracy requirements. At present, there are no reports of direct measurements of the blood flow velocity field at the location of carotid artery stenosis involving biological measurements or in vitro physical experiments. Due to the lack of measured data, numerical simulation studies have highlighted two contradictory views, namely, in one view, the radial sectional velocity of blood flowing across the stenosis location still exhibits a parabolic distribution [11], whereas the other view holds that a parabolic distribution form is not fully developed at the stenosis location [12]. WSS estimations based on these two distributions typically differ by more than 40%. Hence, it is necessary to carry out flow field measurements at the location of vascular stenosis to accurately understand the characteristics of the flow field.

To this end, in this study, a 3D printed model based on real configuration data was adopted to simulate the stenotic blood flow caused by carotid plaques, and a high-resolution flow velocity measurement technique (spatial resolution: up to 1 μm), i.e., microparticle image velocimetry (micro-PIV), was applied to conduct in vitro full velocity field measurements to reveal the flow field characteristics of carotid artery stenosis. On this basis, a numerical simulation study (Fluent; finite volume method) was carried out to reveal the sectional velocity distribution characteristics at the stenosis location. This study aimed (i) to provide support to accurately understand the WSS of carotid artery stenosis and (ii) to propose a reliable method for the study of the flow and shear fields under various blood flow conditions.

Materials And Methods

Three-dimensional reconstruction of carotid artery stenosis and measurement of the blood flow velocity and viscosity.

A computed tomography (CT) scanner (SOMATOM Spirit, Germany) was employed to obtain shape data pertaining to blood vessels near carotid plaques in clinical patients, and coronary and sagittal images of carotid arteries were generated in Mimics software (ver. 20.0) to construct a three-dimensional carotid

artery vascular model. The resultant blood vessel model was smoothed (smoothing coefficient 0.85) in 3-Matic software (ver. 12.0). The average blood flow velocities at the entrance and two exits of the carotid artery model were measured with a colour Doppler ultrasound monitor (Figure 9 (a)). The patient blood viscosity measured with a blood viscometer reached 3.85 mPa·s.

Physical simulation experiment

In carotid artery stenosis blood vessel simulation model preparation, a 3D printer (Zhongrui SLA600, China) was employed to convert the determined three-dimensional geometric model of the blood vessel into a solid simulation model (a layer thickness of 0.1 mm, and the material was transparent photosensitive resin) (Figure 9 (b)).

The physical experiment method in this study relied on a peristaltic pump (YZ1515, China) (rotating speed: 100 r/min; flow rate: 276 mL/min) to provide the power required for fluid flow. A latex tube (inner diameter: 5 mm) was adopted to connect the inlet of the experimental model to the peristaltic pump. A micro-PIV system (Lavision, Germany) was applied to realize velocity field measurement. Fluoro-Max red fluorescent dye (USA) with a peak particle size of 1 μm was employed to track fluid flow. The experimental fluid comprised a 65% dimethyl sulfoxide aqueous solution containing 0.3% fluorescent particles. The viscosity was 3.72 mPa·s and the density reached 998.2 kg/m^3. A device flow chart is shown in Figure 10. During the test, the experimental liquid was continuously injected into the model through the peristaltic pump. When bubbles were no longer observed in the experimental model, the micro-PIV system was activated to record velocity field data, and Davis software (version 10.0.5) was used to process the measured data.

Numerical simulation calculation

In Fluent software (version 19.0), numerical calculations were performed to obtain a three-dimensional reconstruction of carotid artery stenosis, which was meshed as an unstructured tetrahedral mesh (Figure 11 (a)), with a total of 250685 nodes and 1405028 meshes. The governing equation was the Navier-Stoke equation, and the flow mode was laminar flow. The inlet condition of the blood vessel was a function of the periodic velocity over time. The outlet was defined as a free-flow outlet, and the relative pressure at each outlet was set to zero. Considering the physical experiment and the real heart rate cycle of the human body, the inlet cycle was set to range from 0.2-2.0 s. The aim was to analyse the flow pattern of the flow field in the radial section (black line) at the location of carotid artery stenosis (Figure 11 (b)). The flow channel width was normalized with a standardization-MinMax scaler.

Results

Physical simulation results

In the physical simulation experiment, the flow field velocity at the location of carotid artery stenosis was recorded through the micro-PIV system. When stable periodic flow was established, the maximum

average velocity difference was smaller than 0.05 m/s. A velocity cloud chart and radial cross-sectional velocity distribution curve at the location of the vascular stenosis are shown in Figures 1 and 2, respectively.

Numerical simulation results

Verification of the numerical simulation accuracy

In the numerical simulation, to verify the numerical calculation accuracy, the pulsation period was first set to coincide with the peristaltic pump period (0.2 s). When stable periodic flow conditions were established, the maximum average velocity difference was smaller than 0.05 m/s. A velocity cloud chart and radial cross-sectional velocity distribution curve at the location of the vascular stenosis are shown in Figures 3 and 4, respectively.

The velocity distribution, maximum velocity, and velocity gradient near the vessel wall were compared between the numerical and physical experimental results. The velocity distributions determined with the above two methods all exhibited the form of a single-peak distribution. The flow velocities at the centre of the blood vessel were similar, and the velocity distribution indicated plateau-like features, with the width accounting for more than 65% of the total flow path. The deviation in the platform velocity measured with both methods was smaller than 20% at three different moments during the same cycle. The velocity gradients calculated based on the obtained data when the velocity significantly decreased were 1.5×10^3 and 1.75×10^3 s^{-1}, respectively. The numerical simulation accuracy was confirmed by the measured data.

Numerical simulation results under typical human heart rate conditions

Combined with the real heart rate of the human body, the average flow velocity at the inlet was set to 0.6 m/s in the numerical simulations, and the period was 0.8 s. When stable periodic flow was established, the maximum average velocity difference was smaller than 0.05 m/s. The systolic velocity surface (Figure 5), velocity cloud (Figure 6) and flow velocity distribution curve (Figure 7) for the radial section at the stenosis location are shown below.

Discussion

In vitro physical simulation and measurement of the vascular flow field

Generally, there are two key aspects of in vitro experimental studies targeting the intravascular flow field: production of the vessel structure model and measurement of the velocity field within the vessel model. First, the following two issues were included during modelling: the acquisition of vascular conformation data and the preparation of a solid blood vessel model. In terms of vessel configuration, early intravascular flow field studies mainly employed simple ideal models. For example, simulation studies of the carotid artery relied on a simple Y-shaped structure, which was convenient but significantly differed

from the actual structure and inevitably led to insufficient flow field simulations [13-14]. For this reason, CT scanning techniques have been widely applied to obtain configuration information of real blood vessels and to accurately restore irregular vascular structures, such as intracranial aneurysms and carotid artery stenosis vessels [9, 15]. In regard to intracranial aneurysms, relatively systematic numerical and physical simulation studies have been carried out based on the actual structure, revealing the effect of stent placement on the haemodynamics occurring within the aneurysm [16]. In terms of carotid stenotic vessels, haemodynamic analysis of the real vessel structure has only been performed via numerical simulation methods, but no physical simulation experiments have been conducted [17]. To transform 3D structural data into solid models suitable for physical experiments, currently, only 3D printing technology can be relied upon to achieve high-precision recovery (a printing accuracy of 0.05 mm) [18], which has been applied to the fabrication of fine structures such as heart and aortic valves [15], but the preparation of vascular models for carotid stenosis research has not been reported. Two types of materials can be chosen to prepare solid models via 3D printing: rigid materials (photosensitive resin, with an elastic modulus of 2000 MPa) and flexible materials (hydrogel, with an elastic modulus of 80 kPa) [19-21]. Although the elasticity of the latter materials are close to that of carotid vessel walls (an elastic modulus of 47.7 kPa), the low transmittance (milky white colour) inhibits observation and measurement of the internal flow field of the model [21-22]. Thus, photosensitive resin is currently the only viable model material to achieve optical measurements of the stenotic flow field.

With regard to blood flow velocity field measurements, the spatial resolution of the measurement technique should be compatible with the physical model scale. To perform flow field analysis, at least 15 velocity data points are commonly measured in practice to yield a straight curve of the measured flow field [23-24]. Therefore, techniques with a resolution higher than 40 μm are required at carotid stenosis sites. The commonly applied clinical flow velocimetry methods, PC-MRI and ultrasound Doppler velocimetry, cannot realize intravascular velocity field measurements due to their low spatial resolution (0.5-1 mm) [6, 8-10, 25]. Echo-PIV with a higher spatial resolution (0.5 mm) relies on the microbubble contrast of tracer particles to measure the velocity field. Measurement of the velocity distribution characteristics in the radial section of the common carotid artery (10 mm in diameter) has been achieved [8-10, 26], but the spatial resolution remains insufficient for the study of the velocity field in stenosis vessels of the carotid artery (with an internal diameter of only approximately 1-3 mm). Currently, the micro-PIV technique with a maximum resolution of 1 μm can meet this requirement, which realizes the study of the velocity field of blood cells in smaller artificial microchannels (100 μm), yielding a parabolic distribution of the instantaneous velocity in the central plane [23, 27]. This technique has not yet been applied in the study of carotid stenosis vessels.

Based on the above discussion, it can be deduced that the combination of 3D printing technology and the micro-PIV technique represents the only feasible technical route to realize flow field measurement of carotid artery stenosis. In this study, this technical route was applied for the first time to achieve flow field measurement in stenotic vessels, and complete velocity field data of blood flowing across the stenosis location were measured within a flow field of 1.5 mm^2 and 60 velocity points per unit length (1 mm) (in

echo-PIV, only 2-3 data points are typically measured [8-9]), which notably improved the resolution and reliability of stenosis velocity measurement.

Radial cross-sectional velocity distribution characteristics of carotid artery stenosis.

The characteristics of the intravascular flow field distribution are fundamental elements of WSS calculations [9, 28]. Before this study, there were no reports on actual measurement of carotid artery stenosis or external flow field measurement, which left the divergence (parabolic and non-parabolic) between the different velocity distributions in numerical simulations unresolved. In this study, physical experiments and numerical calculations were performed to clarify the characteristics of the radial cross-sectional velocity distribution at the location of carotid stenosis: at normal human heart rates (heart rates ranging from 45-120 beats/min), the flow velocities in the central region of the stenosis location were similar and exhibited plateau-like distribution characteristics rather than an uncommon parabolic distribution.

From the available literature, as two common forms of the velocity distribution of blood flow, i.e., parabolic and plateau forms, the former form was mainly encountered in blood flow in healthy vessels and artificial microfluidic channels [6, 8-9, 29], while the latter was mainly found in the blood flow field of stenotic vessels with abrupt changes in vessel diameter [12]. Studies have analysed blood flow in stenotic vessels of carotid arteries via computer simulations, and the characteristics of the blood velocity distribution in the vessel radial cross-section were considered the result of incomplete blood flow development in the vessel [12]. Another numerical simulation study proposed that after blood flows across the location of blood vessel mutation, after a certain distance of a fixed tube diameter (5 times the tube diameter length), the blood velocity distribution completely developed into a parabolic distribution [30]. Therefore, the sudden change in tube diameter caused by carotid plaques might be one of the important factors of the incomplete development of blood flow to form a plateau-like velocity distribution.

WSS estimation at the carotid artery stenosis location

Based on the characteristic plateau-like distribution of the velocity field at the carotid stenosis location, the WSS was calculated as 20.35 Pa considering the maximum velocity gradient near the vessel wall. However, under the premise of a lack of clinical flow field information, the WSS calculated based on the maximum velocity measured and the conventional parabolic distribution (the blue dotted line in Figure 8) [6-9] reached 7.25 Pa. Therefore, the current clinical estimation method of the WSS at the stenosis location could result in a difference up to 60%, which could notably affect the accuracy of mechanical analysis.

A full understanding of the distribution of the blood flow velocity field is very important for a more accurate calculation of the WSS of carotid artery stenosis. However, carotid vessels of different shapes and varying degrees of stenosis might exhibit notably different flow field characteristics [31-32], and clinical conditions do not facilitate comprehensive flow field measurement. To solve this problem, it is necessary to carry out more basic research to clarify the relationship between the plaque shape, flow field

distribution and WSS, and amendments to the calculated WSS should be proposed for clinical stenosis research purposes to achieve accurate calculation.

Conclusions

In this study, based on carotid stenosis vessel data obtained from real patients, an experimental vessel model was fabricated with 3D printing technology for the first time, and physical experiments were conducted by applying the micro-PIV technique to achieve full velocity field measurement at the stenosis location. This study provides experimental validation of numerical simulation results and reveals the characteristics of the flow field distribution at the stenosis location.

The results revealed that when blood flowed across the carotid artery stenosis location, the velocity distribution was not parabolic but rather a plateau-shaped distribution, with a similar flow velocity in the central area (more than 65% of the total flow path). Therefore, the WSS values calculated based on a parabolic velocity distribution and the maximum velocity were nearly 60% lower.

This study provides a reliable method for WSS determination to better understand the vascular stenosis location and facilitate flow and shear force field research. In the future, it is necessary to carry out in-depth research on the relationship between the plaque shape, flow field distribution and WSS, and amendments to the calculated WSS for clinical stenosis should be proposed.

Abbreviations

WSS: Wall shear stress

PC-MRI: Phase-contrast magnetic resonance imaging

echo-PIV: Echo particle image velocimetry

micro-PIV: Microparticle image velocimetry

CT: Computed tomography

Declarations

Author Contributions

Zhiyong Song, Project administration; Writing review and editing. Pengrui Zhu, Writing original draft. Lianzhi Yang, Methodology. Hua Li, Investigation. Zhaohui Liu, Data curation. Ruonan Li, Conceptualization ideas. Weiyao Zhu, Resources.

Funding

This research was funded by National Natural Science Foundation of China General Program, grant number 41871218.

Acknowledgements

We thank the Hainan Provincial People's Hospital for providing the clinical datas for this research.

Conflicts of Interest

The authors declare no conflict of interest.

Consent for publication

Not applicable.

Availability of data and materials

The datasets analyzed during the current study are available from the corresponding author on reasonable request.

References

1. Peiffer, V., Bharath, A. A., Sherwin, S. J. & Weinberg, P. D. A Novel Method for Quantifying Spatial Correlations between Patterns of Atherosclerosis and Hemodynamic Factors. *Journal of Biomechanical Engineering*, **135**, 021023 (2013).
2. Markl, M. *et al.* Co-registration of the distribution of wall shear stress and 140 complex plaques of the aorta. *Magnetic Resonnce Imaging*, **31**, 1156–1162 (2013).
3. Morito, N. *et al.* Increased carotid artery plaque score is an independent predictor of the presence and severity of coronary artery disease. *Journal of Cardiology*, **51**, 25–32 (2008).
4. Siddiqui, A. H. & Hopkins, L. N. Asymptomatic Carotid Stenosis: The Not-So-Silent Disease. *Journal of the American College of Cardiology*, **61**, 2510–2513 (2013).
5. Kwak, B. R. *et al.* Biomechanical factors in atherosclerosis: mechanisms and clinical implications. *European Heart Journal*, **43**, 3013–3020 (2014).
6. Box, F. M. A. *et al.* Reproducibility of wall shear stress assessment with the paraboloid method in the internal carotid artery with velocity encoded MRI in healthy young individuals. *Journal of Magnetic Resonance Imaging: JMRI*, **26**, 598–605 (2007).
7. Reneman, R. S., Arts, T. & Hoeks, A. P. Wall shear stress-an important determinant of endothelial cell function and structure-in the arterial system in vivo. Discrepancies with theory. *Journal of Vascular Research*, **43**, 51–269 (2006).
8. Gates, P. E. *et al.* Measurement of wall shear stress exerted by flowing blood in the human carotid artery: ultrasound doppler velocimetry and echo particle image velocimetry. *Ultrasound in Medicine and Biology*, **44**, 1392–1401 (2018).

9. Zhang, F. X. *et al.* In vitro and preliminary in vivo validation of echo particle image velocimetry in carotid vascular imaging. *Ultrasound in Medicine Biology*, **37**, 450–464 (2011).
10. Du, Y. G. *et al.* Measurements of wall shear stress for blood vessel and its progress in clinical research (review). *Chinese journal of biomedical engineering*, **037**, 593–605 (2018).
11. Wong, K. K. L. *et al.* Computational medical imaging and hemodynamics framework for functional analysis and assessment of cardiovascular structures. *Biomed. Eng. Online*, **16**, 35 (2017).
12. Lu, Y. Pathological mechanism analysis and clinical application study of atherosclerosis based on hemodynamic. PhD thesis. Shandong University. Ji Nan, China. 2020, 3, 20
13. Yu, F. X. *et al.* The comparative study of velocity profiles in carotid artery bifurcation model by numerical simulation calculation and particle imaging velocimetry measurement. *Journal of Luzhou Medical College*, **32**, 214–217 (2009).
14. Ding, Z. R., Wang, K. Q., Li, J. & Cong, X. S. Flow field and oscillatory shear stress in a tuning-fork-shaped model of the average human carotid bifurcation. *Journal of Biomechanics*, **34**, 1555–1562 (2001).
15. Tom, T., Tal, G. & John, P. Practical clinical applications of 3-D printing in cardiovascular surgery. *Journal of Thoracic Disease*, **9**, 2792–2797 (2017).
16. Li, Y. J., Verrelli, D. I., William, Y., Yi, Q. & Winton, C. A pilot validation of CFD model results against PIV observations of haemodynamics in intracranial aneurysms treated with flow-diverting stents. *Journal of Biomechanics*, **100**, 109590 (2020).
17. Azar, D. *et al.* Geometric determinants of local hemodynamics in severe carotid artery stenosis. *Computers in Biology and Medicine*, **114**, 103436 (2019).
18. Herpel, C. *et al.* Accuracy of 3D printing compared with milling — A multi-center analysis of try-in dentures. *Journal of Dentistry*, **110**, 103681 (2021).
19. Lin, G. *et al.* Photocuring kinetics properties of hybrid UV-curing resin for 3D printing. *Journal of Materials Engineering*, **47**, 143–150 (2019).
20. Arianna, D., Fernández, P. M., Gordon, B., Gianluca, T. & Marta, R. 3D Printing and Electrospinning of Composite Hydrogels for Cartilage and Bone Tissue Engineering. *Polymers*, **10**, 285 (2018).
21. Wang, J. Y. Computer-aided simulation-based studies on mechanical properties of the materials for blood vessel 3D-printing. *Chinese Journal of Applied Mechanics*, **6**, 1379–1383 (2019).
22. Liu, X. Y., Ju, G. & Kelimu, M. CT-based 3D reconstruction of cerebral aneurysm and the hemodynamic characteristics of its blood flow field. *Journal of Interventional Radiology*, **25**, 635–639 (2016).
23. Lima, R., Wada, S., Takeda, M., Tsubota, K. I. & Yamaguch, T. In vitro confocal micro-PIV measurements of blood flow in a square microchannel: The effect of the haematocrit. *Journal of biomechanics*, **40**, 2752–2757 (2007).
24. Fu, Y. *et al.* Micro-PIV measurements of the flow field around cells in flow chamber. *Journal of Hydrodynamics*, **27**, 562–568 (2015).

25. Wise, R. G., Al-Shafei, A., Carpenter, T. A., Hall, L. D. & Huang, L. H. Simultaneous measurement of blood and myocardial velocity in the rat heartby phase contrast MRI using sparse q-space sampling. *Journal of Magnetic Resonance Imaging*, **22**, 614–627 (2005).
26. Kawachi, T., Malkin, R., Takahashi, H. & Hiroshige, K. Prototype of an Echo-PIV Method for Use in Underwater Nuclear Decommissioning Inspections. *Journal of Flow Control, Measurement and Visualization*, **07**, 28–43 (2019).
27. Kvon, A., Lee, Y. H., Cheema, T. A. & Park, C. W. Development of dual micro-PIV system for simultaneous velocity measurements: optical arrangement techniques and application to blood flow measurements. *Measurement Science and Technology*, **25**, 075302 (2014).
28. Park, C. S., Song, R., King, S. H. & Lee, J. Fabrication of artificial arteriovenous fistula and analysis of flow field and shear stress by using μ-PIV technology. *Journal of Mechanical Science and Technology*, **30**, 5503–5511 (2016).
29. Zhu, Y. H., Qian, M., Niu, L. L., Zheng, H. & Lu, G. Measurement method of arterial shear stress of rats model based on ultrasonic particle imaging velocimetry. *Journal of Biomedical Engineering*, **31**, 1355–1360 (2014).
30. Jiang, W. T., Fan, Y. B., Zou, Y. W. & Chen, J. K. Numerical study on the influence of a symmetrical stenosis at the carotid sinus on the flow in the carotid bifurcation. *Chinese Journal of Theoretical and Applied Mechanics*, **38**, 270–274 (2006).
31. Lu, M. M. *et al.* Shape and Location of Carotid Atherosclerotic Plaque and Intraplaque Hemorrhage: A High-resolution Magnetic Resonance Imaging Study. *Journal of Atherosclerosis and Thrombosis*, **26**, 720–727 (2019).
32. Thomas, J. B. *et al.* Variation in the carotid bifurcation geometry of young versus older adults: implications for geometric risk of atherosclerosis. *Stroke*, **36**, 2450–2456 (2005).

Figures

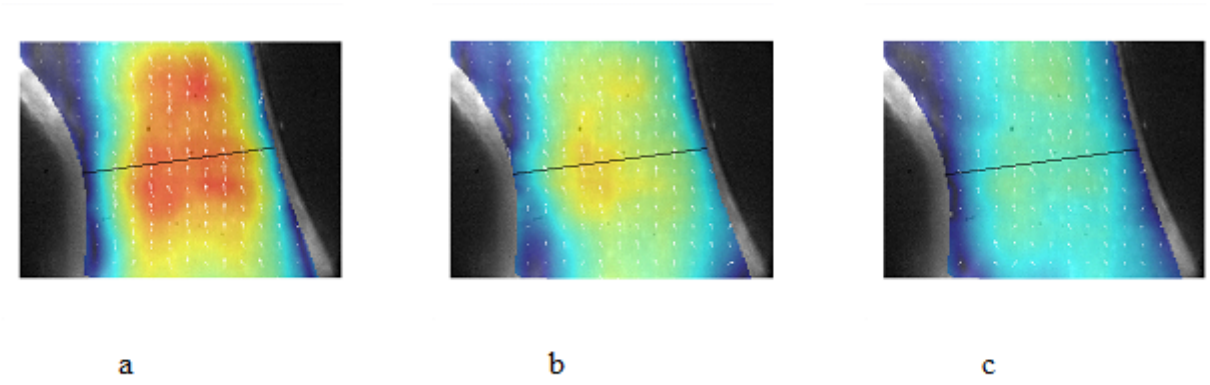

Figure 1

Cloud diagram of the radial sectional velocity at the stenosis location via physical simulations: (a) systolic velocity; (b) flat velocity; (c) diastolic velocity

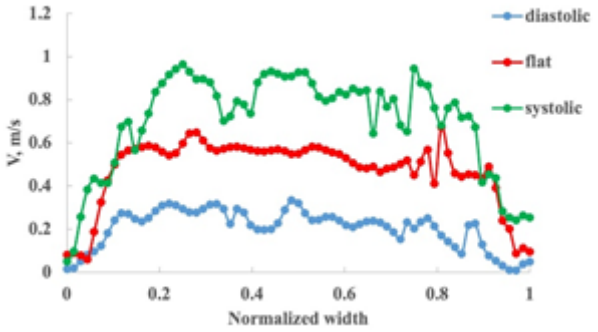

Figure 2

Physical simulation of the radial sectional velocity of carotid artery stenosis

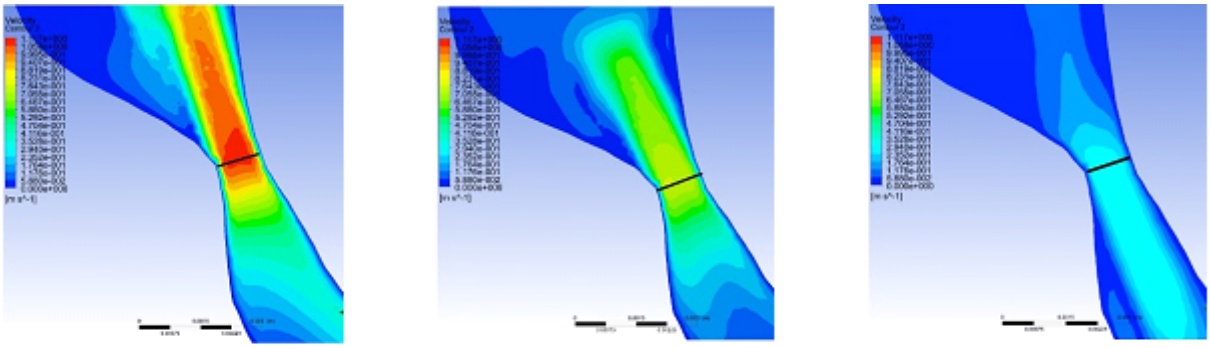

Figure 3

Numerical simulation-based cloud diagram of the radial sectional velocity at the stenosis location: (a) systolic velocity; (b) flat velocity; (c) diastolic velocity

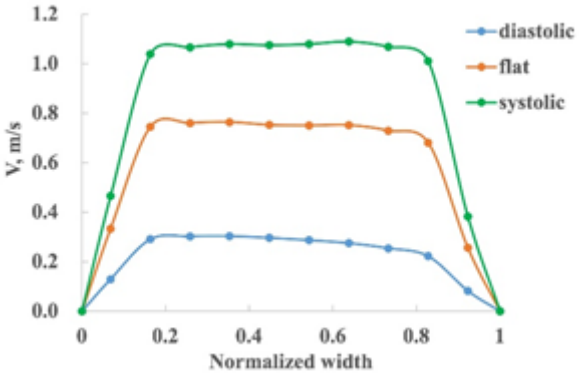

Figure 4

Numerical simulation of the radial sectional velocity of carotid artery stenosis

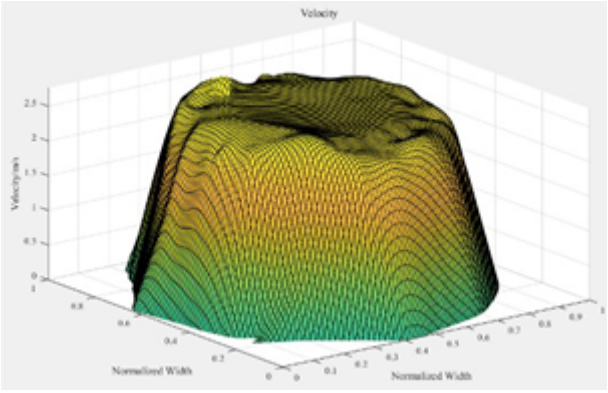

Figure 5

Systolic velocity in the radial section at the location of carotid artery stenosis

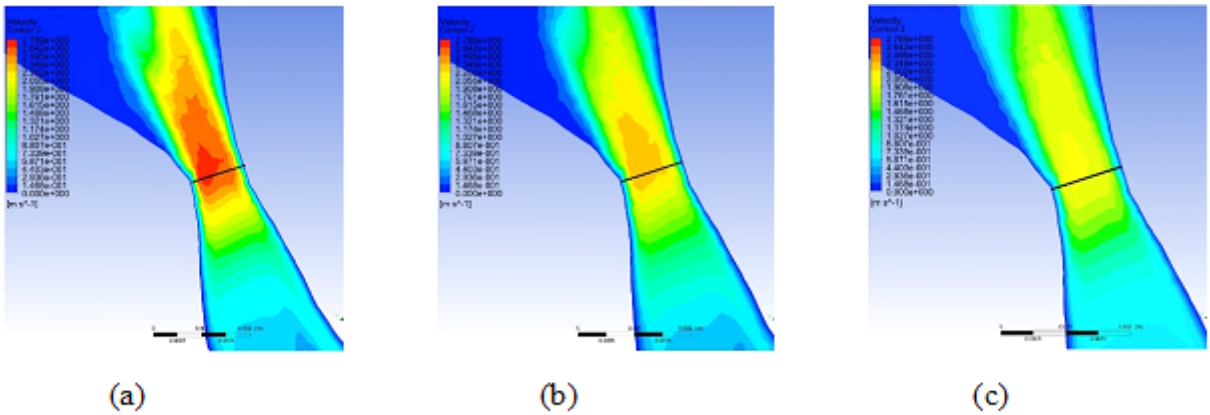

Figure 6

Radial sectional velocity cloud diagram at the stenosis location under real human simulation conditions: (a) systolic velocity; (b) gentle velocity; (c) diastolic velocity

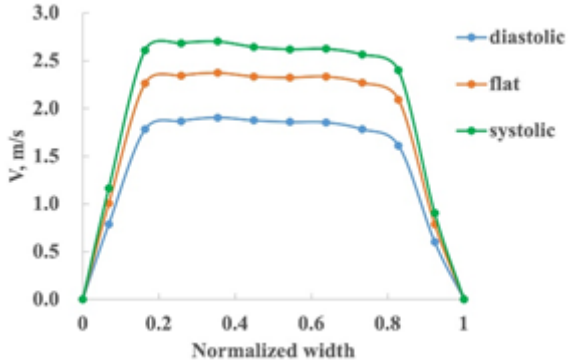

Figure 7

Radial sectional velocity at the stenosis location under real human simulation conditions

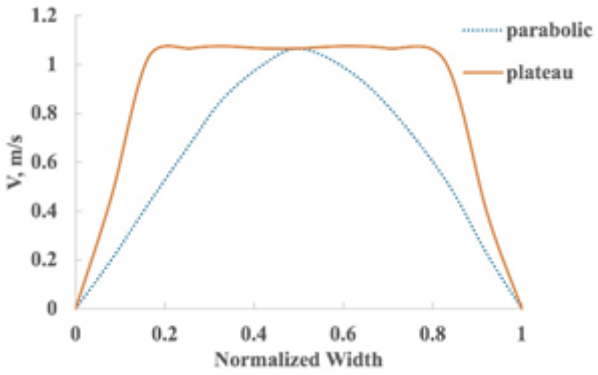

Figure 8

Distribution characteristics of the parabolic and platform velocity distributions based on the same maximum velocity

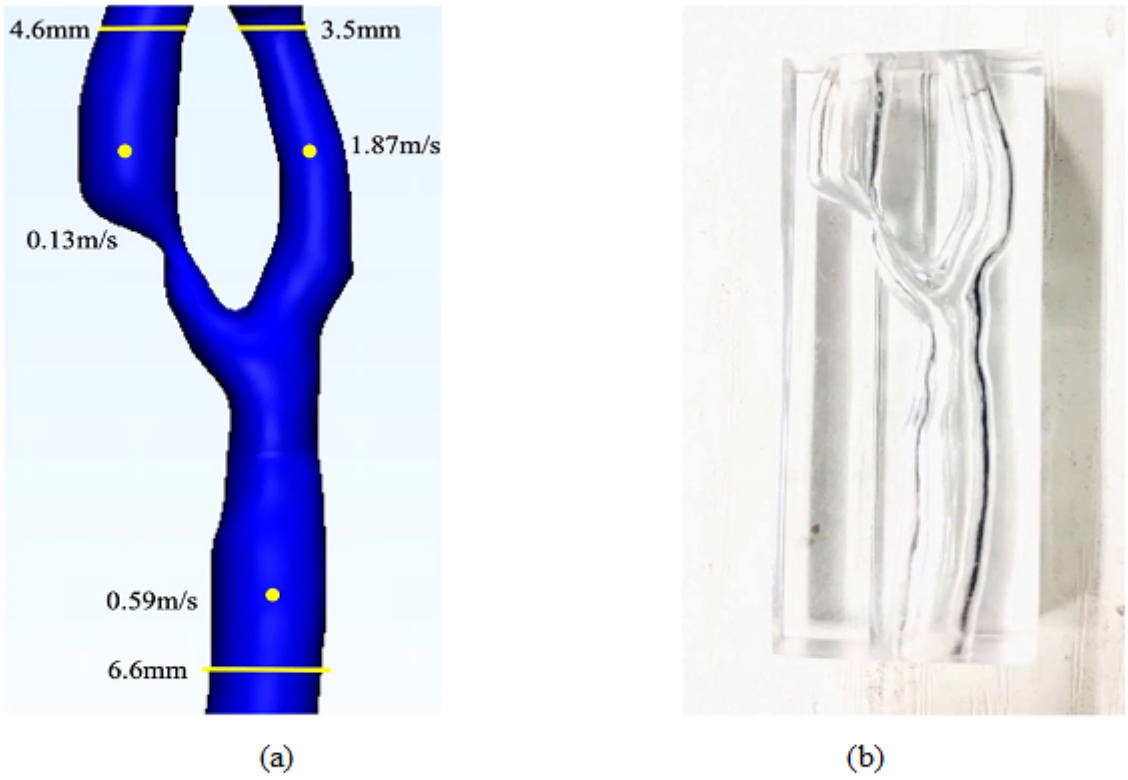

Figure 9

(a) Three-dimensional reconstruction of a carotid artery stenosis vessel, and diameter and flow rate at the blood vessel inlet and outlet. (b) 3D printed simulation model.

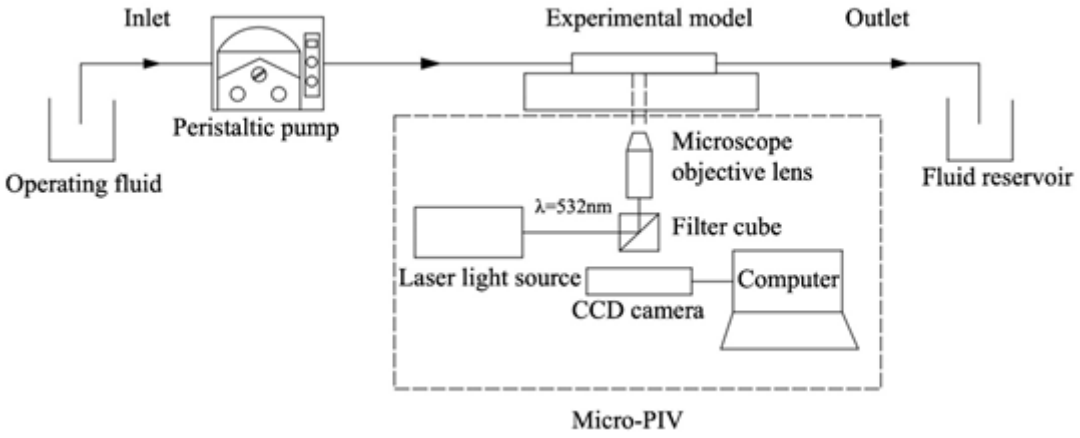

Figure 10

Flow chart of the physical experimental device

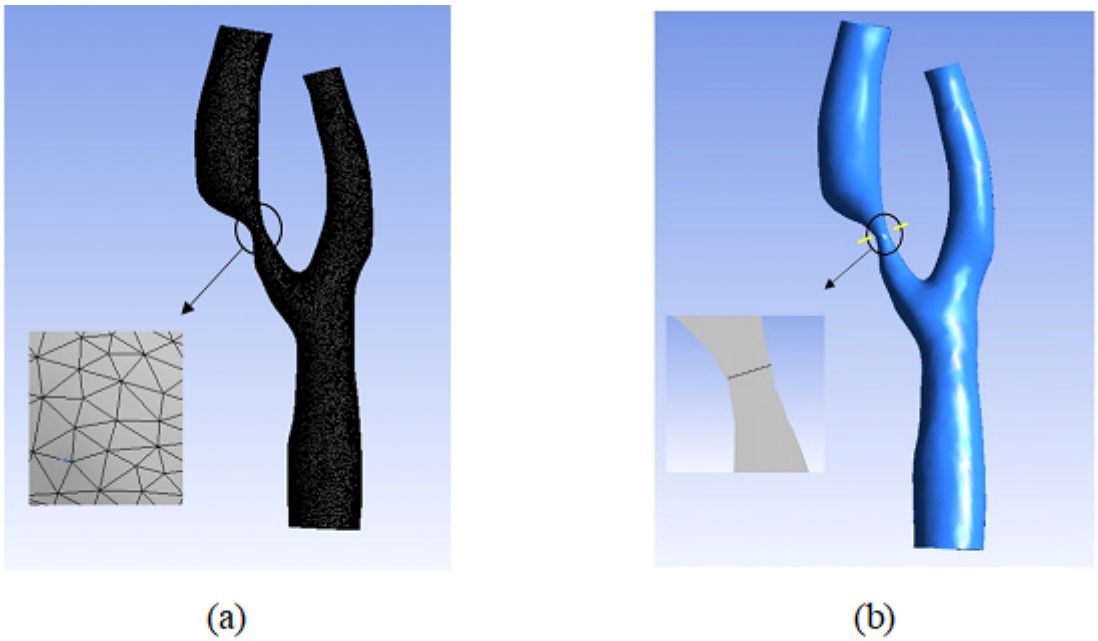

Figure 11

(a) Carotid artery model meshing, (b) carotid artery stenosis location radial section (black line)